PCCP
Physical Chemistry Chemical Physics

Accepted Manuscript

This article can be cited before page numbers have been issued, to do this please use: E. Pean, S. Dmitrov, C. De Castro and M. L. Davies, *Phys. Chem. Chem. Phys.*, 2020, DOI: 10.1039/D0CP04950F.

This is an Accepted Manuscript, which has been through the Royal Society of Chemistry peer review process and has been accepted for publication.

Accepted Manuscripts are published online shortly after acceptance, before technical editing, formatting and proof reading. Using this free service, authors can make their results available to the community, in citable form, before we publish the edited article. We will replace this Accepted Manuscript with the edited and formatted Advance Article as soon as it is available.

You can find more information about Accepted Manuscripts in the Information for Authors.

Please note that technical editing may introduce minor changes to the text and/or graphics, which may alter content. The journal's standard Terms & Conditions and the Ethical guidelines still apply. In no event shall the Royal Society of Chemistry be held responsible for any errors or omissions in this Accepted Manuscript or any consequences arising from the use of any information it contains.

ROYAL SOCIETY OF CHEMISTRY

rsc.li/pccp

ARTICLE

DOI: 10.1039/D0CP05233C

Interpreting Time-Resolved Photoluminescence of Perovskite Materials

Received 00th January 20xx,
Accepted 00th January 20xx

DOI: 10.1039/x0xx00000x

Emmanuel V. Péan[a], Stoichko Dimitrov[b], Catherine S. De Castro[c] and Matthew L. Davies[a,d]

Time-resolved photoluminescence (TRPL) spectroscopy is a powerful technique to investigate excited charge carrier recombinations in semiconductors and molecular systems. The analysis of the TRPL decays of many molecular systems (*e.g.* molecules and organic materials) is usually fairly straightfoward and can be fitted with an exponential function allowing extraction of the rate constants. Due to the non-excitonic nature of charge carriers in lead halide perovskite materials coupled with the presence of localised trap states in their band-gap, the TRPL of these materials is much more complicated to interpret. Here we discuss two models used in the literature to simulate charge carrier recombinations and TRPL in perovskites. These models consider the bimolecular nature of direct electron-hole recombination but differ in their treatment of trap-mediated recombination with one model describing trapping as a monomolecular process whereas the other as a bimolecular process between free carriers and the available trap states. In comparison, the classical analysis of perovskite TRPL decay curves (using a sum of exponentials) can lead to misinterpretation. Here we offer some recommendations for meaningful measurements of lead halide perovskite thin-films. The fluence dependence as well as charge carrier accumulation due to incomplete depopulation of all photoexcited carriers between consecutive excitation pulses are discussed for both models.

Introduction

Since their first use in solar cells in 2009, lead halide perovskites have been employed in wide variety of solar cell architectures leading to an impressive 25.5% power conversion efficiency (PCE) in 2020[1]. Further improvement of the PCE may require enhancing the extraction of the excited charge carriers (electrons and holes) from the perovskite layer to the electron and hole transport layers and reducing the recombination rate of these carriers. Charge carrier recombination generally happens through the direct recombination of an electron and a hole or mediated by defect-induced trap states[2]. These trap states, through their formation and passivation, are also believed to be responsible for the instability and subsequent degradation of the perovskite[3–7]. Extracting information related to these trap states such as their concentration and the trapping rate constant is thus essential in order to compare samples and devices, and improvement of perovskite solar cells.

Time-resolved photoluminescence (TRPL) spectroscopy is a powerful technique that has been employed to study charge carrier recombination kinetics of photoluminescent materials[8–10]. TRPL measures the radiative electron-hole recombination after absorption of a short light excitation pulse (typically of the order of the ps). The TRPL decay obtained is affected by the different competitive radiative and non-radiative recombination processes happening in a system, as well as its environment, and is therefore useful for extracting information related to these processes. TRPL is usually measured using time-correlated single photon counting (TCSPC) in which the sample is periodically excited by a pulsed laser and the sample emission is measured at the desired wavelength. Ideally, after each excitation pulse, 0 or 1 photon is measured, thus generally requiring millions to billions of excitation pulses to obtain an adequate signal to noise ratio (S/N). The TRPL intensity I_{TRPL} measured after P pulses is thus the sum of the TRPL intensity I_{TRPL}^{p} after each excitation pulse p:

$$I_{TRPL}(t) = \sum_{p=1}^{P} I_{TRPL}^{p}(t) \quad (1)$$

TRPL decays have been classically fitted with a sum of exponential decays $A_i e^{-t/\tau_i}$ (A_i and τ_i are respectively the amplitude and lifetime of component i)[11]:

$$I_{TRPL}(t) = \sum_{i}^{n} A_i e^{-t/\tau_i} \quad (2)$$

When applied to perovskite materials, a bi-exponential ($n = 2$) fit is generally done and the two components are usually assigned to trap-mediated recombination (shorter lifetime τ_1) and radiative recombination (longer lifetime τ_2)[12–15]. For perovskite layers in contact with an electron or hole transport material, the faster component has been linked to charge carrier extraction from the perovskite to the transport material[16–21]. The amplitude of each exponential component is usually attributed to the contribution of each process whereas the lifetime indicates the rate of the process[17,19]. However, this model does not consider the dependence of the recombination processes on the excited charge carrier concentration in perovskites.

Here, two models considering direct electron-hole recombination as well as trap-mediated recombination in homogenous perovskite systems are investigated. For most perovskite thin films for solar cells (*i.e.* < *ca.* 200 nm thick),

[a] SPECIFIC IKC, Materials Research Centre, College of Engineering, Swansea University Bay Campus, Fabian Way, Swansea SA1 8EN, UK
[b] School of Biological and Chemical Sciences, Queen 58 Mary University of London, London E1 4NS, UK
[c] KAUST Solar Center KSC, Al-Kindi Bldg (5), Level 3, Room 3204-WS15, Thuwal 23955-6900, Kingdom of Saudi Arabia
[d] School of Chemistry and Physics, University of KwaZulu-Natal, Durban, RSA
† Footnotes relating to the title and/or authors should appear here.
Electronic Supplementary Information (ESI) available: [details of any supplementary information available should be included here]. See DOI: 10.1039/x0xx00000x

carrier diffusion can be assumed much faster than recombination such that the charge carriers can be considered homogenously distributed in the film after photoexcitation (**Note S1**). In such films, the photoexcited charge carrier concentration N_0 generated by an excitation pulse of fluence I_0 (in photons/cm²) is[22]:

$$N_0 = \frac{I_0 A}{D} \quad (3)$$

where A and D are respectively the film absorptance and thickness. Since the carrier concentration N_0 and the excitation fluence I_0 are proportional, they are used interchangeably in this work. At room temperature, the excitons quickly dissociate due to their low binding energy[23], leaving Δn_e electrons in the conduction band (CB) and Δn_h holes in the valence band (VB). The total excited electron $n_e(t)$ and hole $n_h(t)$ concentrations in the conduction (CB) and valence (VB) bands at time t are then:

$$n_e(t) = \Delta n_e(t) + n_0 \quad (4)$$

$$n_h(t) = \Delta n_h(t) + p_0 \quad (5)$$

where n_0 and p_0 are respectively the N-type and P-type doping concentrations which may originate from crystal impurities or point defects, and (intrinsic carriers are ignored due to their low concentration — $\sim 10^4\ cm^{-3}$ at 300K (**Note S1**) — compared to the doping and photoexcited concentrations considered here). Here, we describe three of the recombination processes commonly considered in the literature: band-to-band, non-radiative bimolecular and trap-mediated recombination.

Recombination processes

Bimolecular recombination

Band-to-band recombination is a radiative process during which an excited electron directly recombines with a hole in the VB. Due to the low exciton binding energy in perovskites, excited electrons and holes are uncoupled and their recombination is bimolecular, that is a second order process with a rate dependent on both charge carriers concentrations[2,24,25]. The contribution of this recombination process to the change in the charge carrier concentrations over a small period of time dt is thus equal to the product of the radiative band-to-band recombination rate constant k_R, and the electron n_e and hole n_h concentrations[2,24,25]:

$$\left[\frac{dn_e}{dt}\right]_R = \left[\frac{dn_h}{dt}\right]_R = -k_R n_e(t) n_h(t) \quad (6)$$

Photon recycling, during which emitted photons by the system are re-absorbed before they escape it, has been previously observed in direct band-gap semiconductors with a high absorption coefficient and a small Stoke shift (small difference between emission and absorption maxima), such as perovskites [2,26–28]. As absorption is a much faster process than recombination (~fs versus to ~ns), carriers leading to photon recycling can be assumed to not have recombined. The observed radiative rate constant k_R is thus a fraction of the internal radiative rate constant [2,26,29].

DOI: 10.1039/D0CP05049F

The TRPL intensity measured corresponds to the number of photons emitted by the system studied and is thus equal to:

$$I_{TRPL}(t) = k_R n_e(t) n_h(t) \quad (7)$$

It has been suggested that shallow trap state-mediated recombination and trap-state mediated Auger recombination may lead to non-radiative bimolecular recombination of charge carriers at rate[2,25,26]:

$$\left[\frac{dn_e}{dt}\right]_N = \left[\frac{dn_h}{dt}\right]_N = -k_N n_e(t) n_h(t) \quad (8)$$

where k_N is the non-radiative bimolecular rate constant. As both radiative (**Equation 6**) and non-radiative (**Equation 8**) bimolecular recombination processes depend on the electron and hole concentrations, they can be summed as the bimolecular contribution of rate constant k_B:

$$\left[\frac{dn_e}{dt}\right]_B = \left[\frac{dn_h}{dt}\right]_B = -\underbrace{(k_N + k_R)}_{k_B} n_e(t) n_h(t) \quad (9)$$

Trap-mediated recombination

Trap-mediated recombination, also known as Shockley-Read-Hall recombination can be described as a non-radiative bimolecular process between one carrier type and the available trap states[2,25]. In the case of electron trapping, the trapping contribution is proportional to the product of free electrons n_e and available trap states concentrations $N_T - n_t$, where N_T is the concentration of trap states and n_t is the concentration of trapped electrons occupying these states[2,25]:

$$\left[\frac{dn_e}{dt}\right]_T = -\left[\frac{dn_t}{dt}\right]_T = -k_T n_e(t)[N_T - n_t(t)] \quad (10)$$

where k_T is the electron trapping rate constant. The detrapping of an electron through its recombination with a hole in the VB can be described as a non-radiative bimolecular process between trapped electrons and free holes[2,25]:

$$\left[\frac{dn_t}{dt}\right]_D = \left[\frac{dn_h}{dt}\right]_D = -k_D n_t(t) n_h(t) \quad (11)$$

Where k_D is the detrapping rate constant. In the steady-state regime and if the trap state concentration is much higher than the photoexcited carrier concentration, the electron and hole concentrations can be assumed equal at all time and trap-mediated recombination can be described as a monomolecular processes[30–32]:

$$\left[\frac{dn_e}{dt}\right]_T = \left[\frac{dn_h}{dt}\right]_T = -k_T n_e(t) = -k_T n_h(t) \quad (12)$$

Auger recombination is not discussed here as it has been suggested that it only occurs at very high light fluences (above *ca.* 10 sun illumination) and should therefore be negligible in

PSCs under normal operation illumination conditions and in particular TRPL measurements conditions [33]. Electron detrapping back to the CB, which has been shown to lead to delayed fluorescence (DF) [34,35] could also influence the decay kinetics, however, our aim here is highlight complications with typical analysis found in the literature where commonly DF is not considered.

TRPL kinetic models

In perovskite films, both direct and trap mediated recombination determine the overall charge recombination dynamics. Here we discuss modelling of the TRPL decays with two possible models; the bimolecular-trapping (BT) model and the bimolecular-trapping-detrapping (BTD) model (**Figure 1)**. Both models consider bimolecular recombination of charge carriers but differ in their treatment of trap-mediated recombination.

The BT model assumes the electron and hole concentration equal at all time (*i.e.* $n_e(t) = \Delta n_e(t) = n_h(t) = \Delta n_h(t) = n(t)$) and monomolecular trap-mediated recombination (**Figure 1a**). The rate equation for the BT model is thus build upon **Equations 9** & **12** which give[24,31,36]:

$$\boxed{\frac{dn}{dt} = -\underbrace{k_T n(t)}_{T(t)} - \underbrace{k_B n^2(t)}_{B(t)}} \quad (13)$$

where $T(t)$ and $B(t)$ are the trapping and bimolecular contributions to the change in the charge carrier concentration at time t.

For TCSPC decay analysis, this differential equation is solved with the condition that each excitation pulse p generates N_0 carriers which adds up to any carriers present in the bands just before the pulse. The initial carrier concentration $n^p(t=0)$ of pulse p is thus:

$$\boxed{n^p(t=0) = N_0 + n^{p-1}(RP)} \quad (14)$$

where $n^{p-1}(RP)$ corresponds to the carrier concentration just before excitation pulse p and RP is the excitation repetition period. We assume that TCPSC experiments are started with a film with no free carriers *i.e.* $n^{p=1}(0) = N_0$ (this can be ensured by keeping the sample in the dark for long enough time so that most carriers have recombined).

As per **Equation 7**, the TRPL intensity measured as a function of time after excitation pulse p is given by:

$$\boxed{I^p_{TRPL}(t) = k_R\big(n^p(t)\big)^2} \quad (15)$$

Values of the different rate constants from the literature obtained using the BT model are reported in **Table 1**.

Contrary to the BT model, the BTD model considers trapping and detrapping as bimolecular processes (depicted in **Figure 1b**) and as such it builds upon **Equations 10** & **11**. The electron and hole concentrations are not always equal and so the rate equations for both carrier types and the trapped carrier concentration needs to be solved. Within this model, trapping and detrapping is believed to be mediated by deep trap states while non-radiative bimolecular recombination is mediated by shallow trap states[2]. In the case of electron trapping and considering p-type doping (*i.e.* $n_e = \Delta n_e$ and $n_h = \Delta n_h + p_0$) (as predicted for methylammonium lead iodide (MAPI) using first principle calculations[37]), **Equations 9**, **10** & **11** give the following set of rate equations[2,25,38,39]:

$$\boxed{\frac{d\Delta n_e}{dt} = -\underbrace{k_B \Delta n_e(t)[\Delta n_h(t) + p_0]}_{B(t)} - \underbrace{k_T \Delta n_e(t)[N_T - n_t(t)]}_{T(t)}} \quad (16)$$

$$\boxed{\frac{dn_t}{dt} = \underbrace{k_T \Delta n_e(t)[N_T - n_t(t)]}_{T(t)} - \underbrace{k_D n_t(t)[\Delta n_h(t) + p_0]}_{D(t)}} \quad (17)$$

$$\boxed{\frac{d\Delta n_h}{dt} = -\underbrace{k_B \Delta n_e(t)[\Delta n_h(t) + p_0]}_{B(t)} - \underbrace{k_D n_t(t)[\Delta n_h(t) + p_0]}_{D(t)}} \quad (18)$$

where $B(t)$, $T(t)$ and $D(t)$ are, respectively, the bimolecular, trapping and detrapping contributions to the change in the carrier concentrations.

In TCSPC measurements, the initial carrier concentrations after excitation pulse p generating N_0 carriers are:

$$\boxed{\begin{matrix} \Delta n_e^p(t=0) = N_0 + \Delta n_e^{p-1}(RP) \\ \Delta n_h^p(t=0) = N_0 + \Delta n_h^{p-1}(RP) \\ n_t^p(t=0) = n_t^{p-1}(RP) \end{matrix}} \quad (19)$$

where $\Delta n_e^{p-1}(RP)$, $\Delta n_h^{p-1}(RP)$ and $n_t^{p-1}(RP)$ are the electron, hole and trapped electron concentrations present in the system just before excitation pulse p. As for the BT model, it is assumed that there are no carriers present in the system before the first pulse *i.e.* $\Delta n_e^{p=1}(0) = \Delta n_h^{p=1}(0) = N_0,\ n_t^{p=1}(0) = 0$.

As per **Equation 7**, the TRPL intensity measured after an excitation pulse p is given by:

$$\boxed{I^p_{TRPL}(t) = k_R \Delta n_e^p(t)\big[\Delta n_h^p(t) + p_0\big]} \quad (20)$$

Values of the different rate constants obtained from the literature using the BTD model are reported in **Table 1**.

In this work, the use and limitations of the BT and BTD models are discussed as well as lifetime interpretation of TRPL based on them.

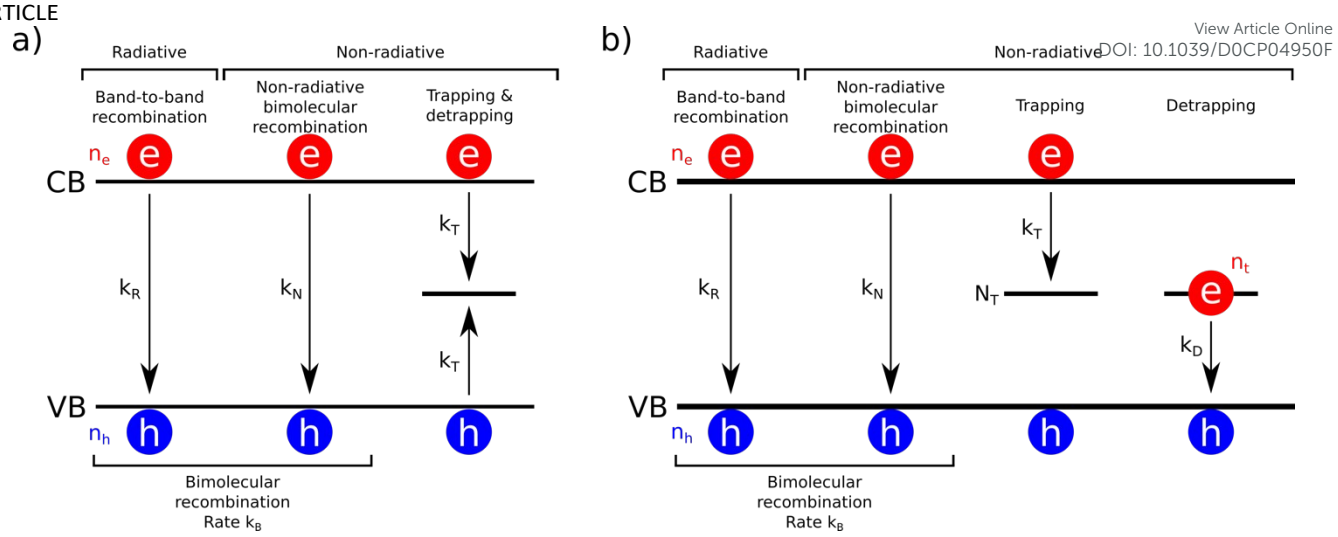

Figure 1: Schematic of the recombination processes considered in the **a)** bimolecular-trapping and **b)** bimolecular-trapping-detrapping models. Excited electrons (concentration n_e) in the conduction band (CB) and holes (concentration n_h) in the valence band (VB) undergo radiative and non-radiative bimolecular recombination at rate constants k_R and k_N respectively (total rate constant k_B). In **a)**, electrons and holes get trapped in trap states at a rate constant k_T. In **b)**, electrons get trapped in trap states (concentration N_T) at a rate constant k_T. Trapped electrons (concentration n_t) can then detrap back to the VB at a rate constant k_D.

Table 1: Recombination rate constants (bimolecular k_B, trapping k_T and detrapping k_D), deep trap states (N_T) and doping (p_0) concentrations for different perovskites obtained using the bimolecular-trapping (left) and bimolecular-trapping-detrapping (right) models [$CH_3NH_3PbI_3$ (MAPI), $CH_3NH_3PbI_{3(1-x)}Cl_{3x}$ (MAPIC), $CH_3NH_3PbBr_3$ (MAPBr)], values taken from literature.

	Bimolecular-trapping model			Bimolecular-trapping-detrapping model					
Perovskite	k_B (10^{-20} cm^3/ns)	k_T (10^{-3} ns^{-1})	Ref.	k_B (10^{-20} cm^3/ns)	k_T (10^{-20} cm^3/ns)	N_T (10^{12} cm^{-3})	p_0 (10^{12} cm^{-3})	k_D (10^{-20} cm^3/ns)	Ref.
MAPI	17	180	24	35	10	60,000	10,000	5	25
	51-220	3-28	40						
	8.1	5	26	26-76	12,000	60	65	80	2*
	92	14	41						
MAPBr	12-20	2.9-1,100	42	Not found					
	7.0	2.5	26						
MAPIC	7.9	≤ 0.5	26	49	~0	< 500	1,000	~0	25

Methodology

We describe here the methods and parameters used to simulate the carrier concentrations and TRPL, as well as details about the fitting of the TRPL decays.

Simulations

Carrier concentrations and TRPL intensity were simulated by following the process described in the block diagram in **Figure S1**, presented for the BT model only. The same process is valid for the BTD model by replacing the equations with **Equations 16-20**. Unless otherwise stated, all carrier concentrations and TRPL decays were calculated after the first excitation pulse only (referred to as the single pulse approximation in the results & discussions section). For the BT model, the carrier concentration was simulated using **Equation 13** and **14** and $k_B = 50 \times 10^{-20}\ cm^3/ns$ and $k_T = 15 \times 10^{-3}\ ns^{-1}$, values consistent with what has been reported for perovskites **(Table 1)**. The TRPL intensity was then simulated using **Equation 15**. For the BTD model, the carrier concentrations were simulated using **Equations 16-18** and the rate constants and the concentrations reported for a pristine MAPI thin film in [2] (* in **Table 1**): $k_B = 26 \times 10^{-20}\ cm^3/ns$, $k_T = 12{,}000 \times 10^{-20}\ cm^3/ns$, $k_D = 80 \times 10^{-20}\ cm^3/ns$, $p_0 = 65 \times 10^{12}\ cm^{-3}$ and $N_T = 60 \times 10^{12}\ cm^{-3}$. The TRPL intensity was then simulated using **Equation 20**. We note that there seems to be two scenarios in the literature, one with fast trapping rate constant and smaller number of traps and one with slower trapping rate constant and much larger number of traps. In this work we focus on the former as we feel it describes best the systems we have encountered. As discussed in the results &

discussions section, TRPL decays resulting from billions of excitation pulses, as the ones experimentally measured, are simulated with only a few hundred excitation pulses until stabilisation of the carrier concentration(s) defined as :

$$\left|n_X^{p-1}(t) - n_X^p(t)\right| \leq 10^{-6} N_0 \quad (21)$$

Excitation pulse p is then assumed representative of the carrier concentration in the system after billions of pulses. This method is referred to as the multiple pulse approximation and allows to greatly reduce the calculation cost. Further details about the calculations can be found in **Note S2**.

The contribution $C(t)$ of a recombination process (*e.g.* $T(t)$ for trapping) corresponds to the rate of charge carriers recombined through such process at a given time t. Over a certain period of time, the total contribution $\bar{C}$, *i.e.* the total number of carriers recombined through this process, is given by:

$$\bar{C} = \int C(t)\, dt \quad (22)$$

The relative contribution $\%C(t)$ of a certain process corresponds to the ratio of carriers recombined through this process to the sum $\sum C(t)$ of all carriers recombined at time t (**Note S3**):

$$\%C(t) = \frac{C(t)}{\sum C(t)} \quad (23)$$

Consequently, we note $\%\bar{C}$ the relative total contribution which corresponds to the percentage of charge carriers recombined through a certain process over a certain period of time.

Since the carrier concentration is not the quantity observed when measuring TRPL, it is necessary to quantify the contribution of each recombination process to the changes in the TRPL intensity. In the BT model (**Equation 15**), the change in the TRPL intensity over a small period of time dt is:

$$\frac{dI_{TRPL}}{dt} = -\underbrace{2k_R n(t) B(t)}_{B_{PL}(t)} - \underbrace{2k_R n(t) T(t)}_{T_{PL}(t)} \quad (24)$$

where $B_{PL}(t)$ and $T_{PL}(t)$ are the bimolecular and trapping contributions to the change in the TRPL intensity. In the BTD model (**Equation 20**), the change in the TRPL intensity over a small period of time dt is:

$$\frac{dI_{TRPL}}{dt} = -\underbrace{k_R B(t)[\Delta n_e(t) + \Delta n_h(t) + p_0]}_{B_{PL}(t)} - \underbrace{k_R T(t)[\Delta n_h(t) + p_0]}_{T_{PL}(t)} - \underbrace{k_R D(t) \Delta n_e(t)}_{D_{PL}(t)} \quad (25)$$

where $B_{PL}(t)$, $T_{PL}(t)$ $D_{PL}(t)$ are respectively the bimolecular, trapping and detrapping contributions to the change in the TRPL intensity.

Fitting

In order to investigate the limitations of the models, fitting was carried out on TRPL decays simulated with the BT and BTD models. With the BT model, the decays were simulated with 512 points (or channels) while 4096 points were used with the BTD model in order to resolve the fast trapping predicted by this model. Prior to fitting, noise simulated from a Poisson distribution was added to emulate experimental conditions (an amount of noise reasonably representative of experimental conditions as shown in **Figure S4**) and the decays were normalised with respect to their initial intensity. The excitation repetition period used (*i.e.* the time window used) was chosen such that $I_{TRPL}(RP)/I_{TRPL}(0) \sim 10^{-4}$ (where I_{TRPL} is the TRPL intensity after the first pulse within the single pulse approximation and after the last pulse determined from **Equation 21** within the multiple pulse approximation) which we think is representative of experimentally measured TRPL decays. Fitting was carried using a least-square minimisation of the free parameters (k_B and k_T for the BT model and k_B, k_T, k_D, p_0 and N_T for the BTD model) (**Note S4**). We considered a "best-case scenario" where the same values of the parameters used in the simulated TRPL decays were used as guess values for the fitting optimisation.

View Article Online
DOI: 10.1039/D0CP05112

Results & discussions

Here we discuss the application of the BT and BDT models to describe TRPL decays of perovskite samples. First discuss the excitation fluence dependence on TRPL after the first excitation pulse (the superscript notation is ignored here for clarity *i.e.* $n_X^{p=1}(t) = n_X(t)$). This is an important topic as TRPL decays are usually reported at a variety of fluences in the literature, making comparisons across the literature difficult. We also discuss the accuracy of the values retrieved from fitting these decays simulated with added noise at different excitation fluences. In the second section, we discuss the importance of allowing recombination of all photoexcited charge carriers for fitting with a single excitation pulse and advise on how to avoid charge accumulation in the systems measured.

Bimolecular-trapping model

Fluence regimes

We investigate the fluence dependence of the BT model by simulating the carrier concentration and TRPL for a wide range of initial carrier concentrations N_0. Within this model, the carrier concentration normalised to its initial value $n(t)/N_0$ (and therefore the normalised TRPL intensity) is observed to decay faster for increasing N_0 (**Figure 2a**, **Note S6**). In order to estimate the effect of trapping and bimolecular recombination on the TRPL decay, we investigate their contribution to the change in the TRPL intensity, $\%\overline{T_{PL}}$ and $\%\overline{B_{PL}}$ respectively. In particular, we note that $\%\overline{T_{PL}}$ and $\%\overline{B_{PL}}$ are respectively lower and higher than the contributions to the change in the carrier concentrations $\%\overline{T}$ and $\%\overline{B}$ as the square of the carrier concentration favours bimolecular contribution, which means that bimolecular recombination has a greater effect on the TRPL profile than trapping (**Figure 2c**).

View Article Online
DOI: 10.1039/D0CP05105

Under low excitation fluence (here $N_0 < 10^{15}\ cm^{-3}$), trapping is the dominant recombination process as $k_T N_0 \gg k_B N_0^2$. This is demonstrated in **Figure 2b** where the trapping contribution $\%T_{PL}$ is close to 100% over the whole time-range studied (blue curves). Consequently, the total trapping contribution $\%\overline{T_{PL}}$ is close to 100% while the total bimolecular contribution $\%\overline{B_{PL}}$ is negligible (**Figure 2c**). In this regime, the BT rate equation and TRPL (**Equations 13** & **15**) can be simplified to:

$$\frac{dn}{dt} \approx -k_T n(t) \Rightarrow I_{TRPL}(t) \propto e^{-2k_T t} \quad (26)$$

The TRPL therefore follows a mono-exponential trend dependent only on the trapping rate constant k_T and does not depend on the initial carrier concentration N_0 (blue curves in **Figure 2a**). The low contribution of bimolecular recombination in this regime may lead to inaccurate determination of the bimolecular recombination rate constant k_B when fitting TRPL. To illustrate this, we simulate TRPL decays at low fluence using the BT model and add some noise to emulate experimental conditions. The decays are then fitted using the same model yielding the accurate value of k_T but an inaccurate value of k_B, even though the correct values of the parameters were used as initial guesses (**Figure 2d**).

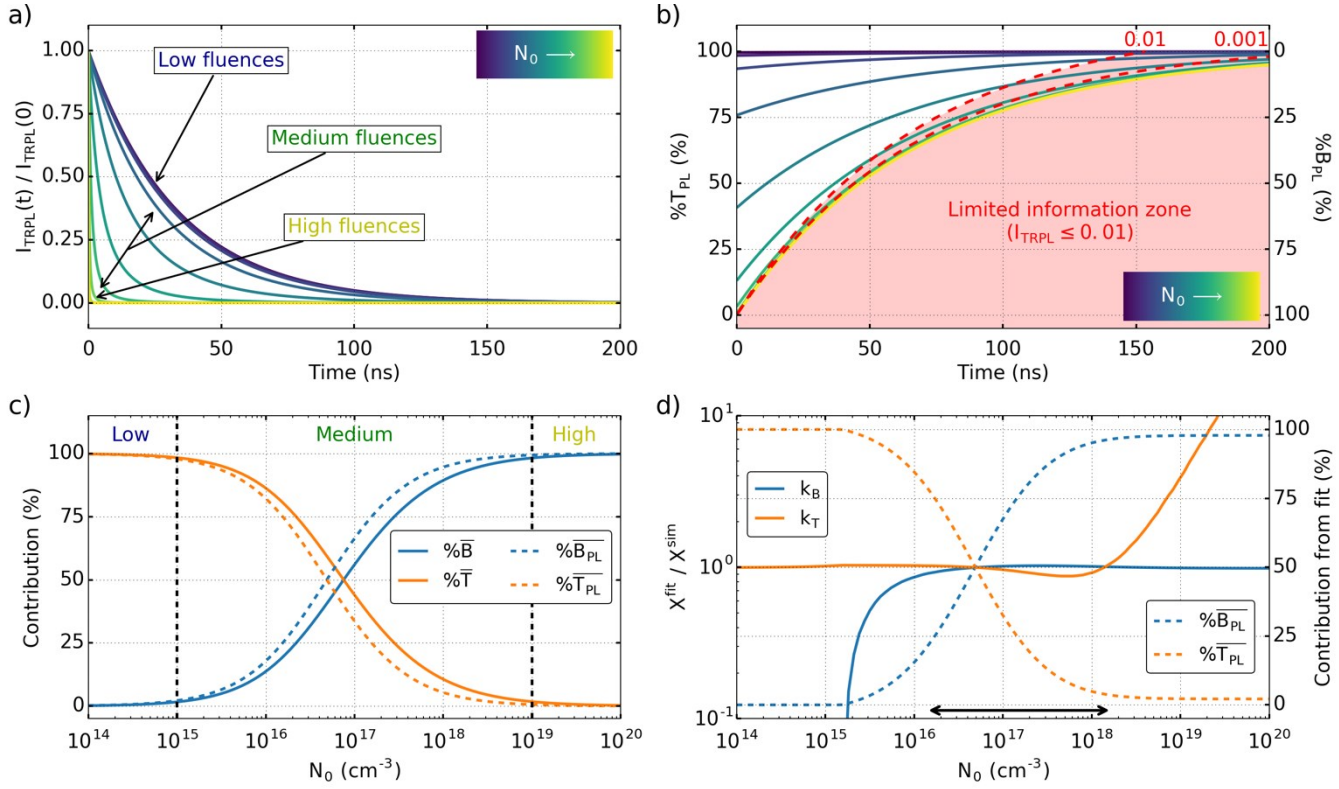

Figure 2: Fluence dependence on the recombination process and the determination of their rate constants as predicted by the bimolecular-trapping model. a) Simulated TRPL decays, **b)** relative trapping $\%T_{PL}$ and bimolecular $\%B_{PL}$ contributions to the change in the TRPL intensity and **c)** total bimolecular and trapping contributions to the change in the carrier concentration ($\%\overline{B}$ and $\%\overline{T}$) and the TRPL intensity ($\%\overline{B_{PL}}$ and $\%\overline{T_{PL}}$) at increasing excitation fluences ($10^{14} cm^{-3} \leq N_0 \leq 10^{20}\ cm^{-3}$). In **b)** the red dashed lines indicate where the associated normalised TRPL intensity becomes lower than 0.01 and 0.001. The red area defines the time for each excitation fluence over which the TRPL intensity is lower than 0.01 and thus where information about trapping may not be recoverable. **d)** Bimolecular k_B and trapping k_T rate constants obtained from fitting TRPL decays with added noise, and normalised to the values used in the simulations ($R^2 > 0.998$). A value of 1 or close to 1 indicates that it is accurately retrieved. The double arrow indicates the fluence range where both rate constants can be retrieved with less than 10 % relative error. The total trapping $\%\overline{T_{PL}}$ and bimolecular $\%\overline{B_{PL}}$ contributions calculated from the fits are also shown as dashed lines.

Under medium excitation fluence ($k_T N_0 \sim k_B N_0^2$, here $N_0 \sim 10^{15} - 10^{19}\ cm^{-3}$), the bimolecular and trapping contributions are comparable, with bimolecular recombinations dominant in the initial decay and trapping dominant in its tail (green curves in **Figure 2b**). The TRPL profile is dependent on the initial carrier concentration (green curves in **Figure 2a**). Since both $\%\overline{T_{PL}}$ and $\%\overline{B_{PL}}$ are non-negligible, it is possible to accurately retrieve both recombination rate constants from the fitting of simulated medium fluence TRPL decays with added noise as shown in **Figure 2d**.

Under high excitation fluence ($k_T N_0 \ll k_b N_0^2$, here $N_0 > 10^{19}\ cm^{-3}$), the bimolecular contribution is initially dominant but quickly decreases as the carrier concentration $n(t)$ decreases while the trapping contribution increases (yellow curves in **Figure 2b**). It may thus be possible to retrieve the trapping rate constant at the tail of the TRPL decay where the carrier concentration is low and $\%T_{PL}$ is high. However,

View Article Online
DOI: 10.1039/D0CP04950F

experimentally measured TRPL decays usually include a certain degree of noise which may limit the determination of the trapping rate constant as the S/N is lower at lower TRPL intensity (*i.e.* at the tail of the decay). For example, the time at which the normalised TRPL intensity reach 0.01 is shown as dashed red lines in **Figure 2b**. Under high fluence, trapping only contributes a few percent of the total recombinations before the TRPL reaches 0.01 normalised intensity in **Figure 2b** (yellow curves). Consequently, fitting TRPL decays simulated at high excitation fluences with added noise yields an accurate value of k_B but not of k_T (**Figure 2d**). Improving the S/N (*e.g.* 0.001 curve in **Figure 2b**) improves the accuracy of the trapping rate determined (**Figure S5** shows the value of k_T and k_B retrieved from fitting for different amount of noise).

The accuracy of the rate constant values retrieved from fitting (at any fluence) can be estimated by calculating the total bimolecular and trapping contributions using these values. For example, in **Figure 2d** the values of the rate constant retrieved from fitting become inaccurate when $\%\overline{B_{PL}}$ and $\%\overline{T_{PL}}$ get close to zero, respectively at low and high fluence, consistent with our previous observations.

The different fluence regimes of the BT model are summarised in **Table S1**.

Incomplete recombination

As TCSPC measurements generally require millions to billions excitation pulses to obtain an appropriate S/N, fitting experimentally measured TRPL by simulating only the first excitation pulse (referred to as the single pulse approximation hereafter) requires that all charge carriers recombine between two consecutive excitation pulses. To illustrate this, we compare the evolution of the carrier concentration after multiple consecutive pulses with excitation repetition periods $RP = 25\ ns$ and $RP = 200\ ns$ (**Figure 3a**). In both cases, the first pulse excites $n^{p=1}(0) = N_0$ carriers. When measured with a $200\ ns$ repetition period, $n^{p=1}(RP) = 0.01\ N_0$ carriers are left in the bands just before the second excitation pulse (red curve). The initial carrier concentration of the second excitation pulse is thus $n^{p=2}(0) = n^{p=1}(RP) + N_0 = 1.01N_0$ leading to a similar variation of the carrier concentration as after the first pulse (**Figure 3a**). The resulting TRPL decay after 10^9 pulses is thus similar to the TRPL decay simulated with only the first excitation pulse (**Figure 3b**) and single pulse fitting can therefore be used. Conversely, with a $25\ ns$ repetition period, $n^{p=1}(RP) = 0.34\ N_0$ carriers are left in the system before the second excitation pulse (purple curve in **Figure 3a**). The higher initial carrier concentration of the second pulse $n^{p=2}(0) = 1.34N_0$ accelerates the recombination due to the higher bimolecular contribution. The TRPL decay obtained after 10^9 pulses is 1.9 times more intense than the single pulse TRPL decay (not shown here) and decays faster due to the higher carrier concentration (**Figure 3b**). Such decay cannot be fitted with a single pulse and would require the simulation of all the excitation pulses. The accumulation of charge carriers in the system continues until as many carriers recombine after an excitation pulse as carriers are generated by the latter (**Figure 3a**):

$$n^p(0) - n^p(RP) = N_0 \quad (27)$$

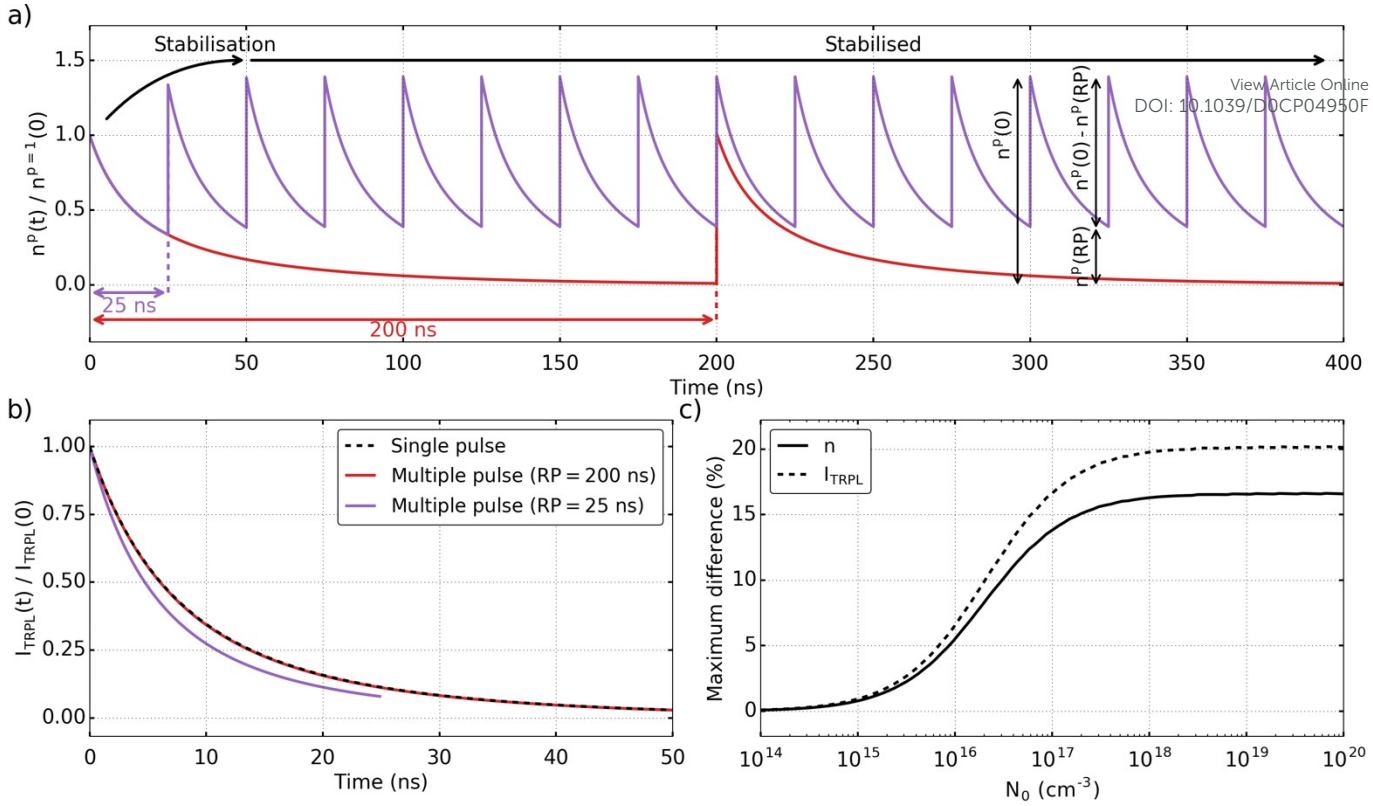

Figure 3: Effect of incomplete depopulation on the carrier concentration and TRPL over time as predicted by the bimolecular-trapping model at medium fluence excitation ($N_0 = 10^{17}\ cm^{-3}$) and different excitation repetition periods ($RP = 200\ ns, 25\ ns$). **a)** Carrier concentration $n^p(t)$ normalised to its initial value after the first excitation pulse $n^{p=1}(0)$ over 400 ns and **b)** normalised TRPL intensity after 10^9 pulses. The TRPL decay simulated after a single pulse is also shown for comparison. **c)** Maximum difference between the single pulse and multiple pulse normalised TRPL and carrier concentration at increasing N_0 (the repetition period was chosen such that $I_{TRPL}(RP)/I_{TRPL}(0) = 0.25$).

This carrier accumulation (CA) does not affect the profile of the TRPL decay at low fluences (as shown in **Figure 3c** & **S6**) as monomolecular recombination does not depend on the carrier concentration (although the increased initial carrier concentration may drive the system in a regime where bimolecular recombination are non-negligible). As the fluence is increased, CA becomes more and more important partially due to the higher contribution of bimolecular recombination (**Figure 3c**).

Assuming that the carrier concentration stabilises over a small fraction of the total number of excitation pulses experimentally required to obtain a good S/N TRPL decay (as suggested by our simulations), it is possible to simulate and fit TRPL decays resulting from billions of excitation pulses by only simulating a small fraction of them and by considering the last simulated pulse to be representative of the system measured (referred to as the multiple pulse approximation hereafter). However, multiple pulse fitting is much slower than single pulse fitting and measuring incomplete decays (*i.e.* without their tail) reduces the range of fluences where k_T and k_B can both be accurately retrieved as discussed in **Note S7**.

It is thus essential to avoid CA in order to use single pulse fitting. This can be ensured by choosing an excitation repetition period such that the TRPL decay reaches zero. The TRPL decay can only reach zero if the TRPL intensity after each pulse I^p_{TRPL} reaches zero by the end of the repetition period as per **Equation 1**:

$$I_{TRPL}(RP) = 0 \Rightarrow I^p_{TRPL}(RP) = 0 \quad (28)$$

Since the TRPL intensity is proportional to the square of the carrier concentration, **Equation 28** implies that the carrier concentrations also reach zero:

$$I^p_{TRPL}(RP) = 0 \Rightarrow n^p(RP) = 0 \quad (29)$$

As per **Equation 27**, this means that the initial carrier concentration of each pulse is $n^p(0) = N_0$ and therefore CA is negligible. It is thus straightforward to avoid CA according to the BT model by choosing an excitation repetition period such that the TRPL decay is fully measured *(e.g.* when I_{TRPL} is at least 0.01% it indicates under 1% of non-recombined charge carriers).

Bimolecular-trapping-detrapping model

Contrary to the BT model, the BTD model does not consider trapping and detrapping to be synchronous. For the following analysis and discussion, we assume that the doping concentration is of the same order of magnitude than the trap state concentration, and that the trapping rate constant is much higher than the bimolecular and detrapping rate constants.

Fluence regimes

We investigate the fluence dependence of the BTD model by simulating the carrier concentration and TRPL for a wide range of initial carrier concentrations. Contrary to the BT model, the BTD model does not predict a straightforward trend of the TRPL profile (**Figure 4a**). We note that over the whole fluence range studied, the total trapping $\%\overline{T}$ and detrapping $\%\overline{D}$ contributions are always equal since as many carriers get trapped and

detrapped, however, their contribution to the change in the TRPL intensity are different as discussed hereafter (**Figure 4c**).

Under low excitation fluence (*i.e.* $N_0 \ll N_T$, here $N_0 < 5 \times 10^{12}\ cm^{-3}$), the hole concentration can be assumed constant and equal to the doping concentration, and therefore the bimolecular contribution has a monomolecular behaviour:

$$B(t) = k_B \Delta n_e(t)[\Delta n_h(t) + p_0] \approx k_B \Delta n_e(t) p_0 \quad (30)$$

As the photoexcited electron concentration is much lower than the trap states concentration, the trap states can be considered empty at all time and the trapping contribution has also a monomolecular behaviour:

$$T(t) = k_T \Delta n_e(t)[N_T - n_t(t)] \approx k_T \Delta n_e(t) N_T \quad (31)$$

The bimolecular and trapping processes are therefore undistinguishable in this regime. Since the hole concentration is constant, the TRPL intensity follows the same trend as the electron concentration and is mono-exponential which shape does not depend on the excitation fluence (**Figure 4a**):

$$I_{TRPL}(t) = p_0 \Delta n_e \propto e^{-(k_B p_0 + k_T N_T)t} = e^{k_M t} \quad (32)$$

View Article Online
DOI: 10.1039/D0CP04950F

where $k_M = k_B p_0 + k_T N_T$. In the present simulations, we assumed $k_T N_T \gg k_B p_0$ and therefore the TRPL decays only depend on the product $k_T N_T$ (other cases are discussed in **Note S8** but **Equation 32** remains valid). This is consistent with the negligible bimolecular $\%\overline{B_{PL}}$ and detrapping $\%\overline{D_{PL}}$ contributions to the change in the TRPL intensity shown in **Figure 4c**. As discussed for the BT model, only k_M can be retrieved from fitting TRPL decays in this regime and therefore any combination of values of k_B, p_0, k_T and N_T yielding the same value k_M are a solution to the fit. We demonstrate this by fitting TRPL decays simulated with the BTD model in the low fluence regime where different sets of values of k_B, p_0, k_T and N_T are retrieved, all yielding the same k_M value (**Note S9**).

As the excitation fluence increases and become close to the trap state concentration, the availability of the trap states needs to be considered and trapping has a bimolecular behaviour leading to non-exponential TRPL profiles.

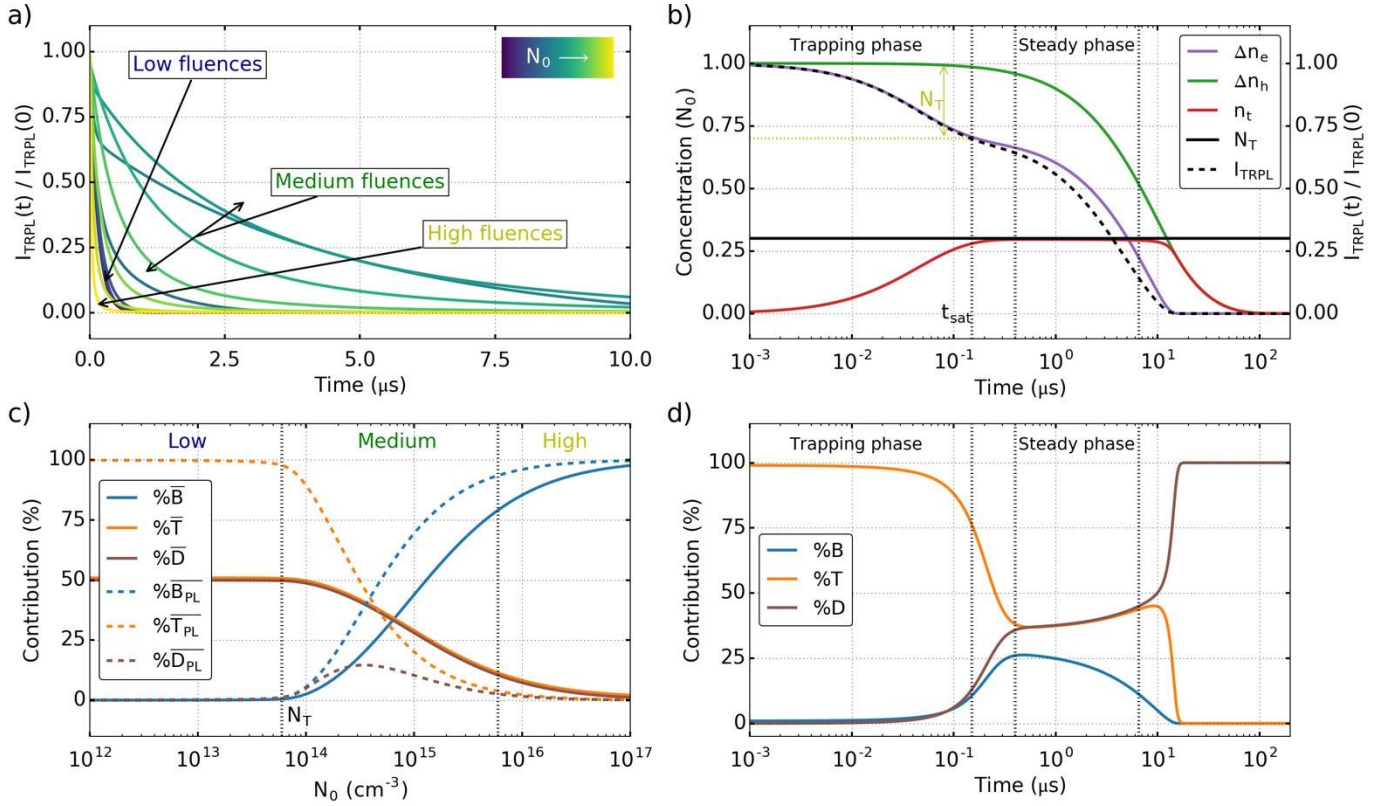

Figure 4: **Fluence effect on the recombination processes predicted by the bimolecular-trapping-detrapping model. a)** TRPL decays and **c)** total bimolecular, trapping and detrapping contributions to the change in the carrier concentrations ($\%\overline{B}$, $\%\overline{T}$, $\%\overline{D}$ respectively, full curves) and TRPL intensity ($\%\overline{B_{PL}}$, $\%\overline{T_{PL}}$, $\%\overline{D_{PL}}$ respectively, dashed curves) at increasing excitation fluences ($10^{12} - 10^{17}\ cm^{-3}$). **b)** Evolution of the photoexcited electron (Δn_e), hole (Δn_h) and trapped electron (n_t) concentrations, and TRPL intensity (I_{TRPL}), and **d)** associated relative bimolecular ($\%B$), trapping ($\%T$) and detrapping ($\%D$) contributions after an excitation pulse generating $N_0 = 2 \times 10^{14}\ cm^{-3}$ (N_T: trap state concentration).

ARTICLE

Under medium excitation fluence (*i.e.* $N_T < N_0 < \sim 100 N_T$, here $N_0 \sim 6 \times 10^{13} - 6 \times 10^{15}\ cm^{-3}$), the electrons quickly fill the trap states to saturation (**Figure 4b**). The trapping then slows down due to the absence of available trap states and the free electrons can only undergo bimolecular recombination while the high trapped electron concentration leads to an increase of the detrapping contribution (**Figure 4d**). As these processes are slower than trapping, the TRPL decay decrease slows down after about 100 ns in **Figure 4b**. Since the hole concentration can be assumed constant over the initial trapping phase (as previously discussed in the low fluence regime) the TRPL intensity can thus be considered proportional to the electron concentration as observed in **Figure 4b**. The trap state concentration can thus be roughly determined from the difference between the TRPL initial intensity and its intensity at t_{sat} where the TRPL decrease slows down, multiplied by the initial carrier concentration (**Note S10**):

$$N_T \sim [I_{TRPL}(0) - I_{TRPL}(t_{sat})] N_0 \quad (33)$$

The trapping rate constant can also be extracted from the trapping phase by fitting the initial TRPL decay with a mono-exponential function, as long as it remains mono-exponential (*i.e.* that the trap states remain mostly empty, **Note S10**). As the trap states are filled, the detrapping and trapping contributions become equal such that any electron detrapped gets replaced by another electron and the trap states remain full at any time (**Figure 4b & d**). This steady-state continues until the electron concentration becomes low enough that trapping becomes slower than detrapping and the trap states depopulate. As for the low fluence regime, detrapping can happen after the TRPL intensity has reached zero and has therefore a limited contribution to the change in its intensity as shown in **Figure 4c**. Since all the recombination processes are non-negligible in this regime, it is possible to accurately retrieve all the parameters of the model (**Note S9**). However, contrary to the BT model where a set of values gives a very distinct TRPL decay, the BTD model can yield very similar TRPL decays calculated from different sets of values, even over a wide range of fluences as discussed in **Notes S11** & **S12**). It is thus necessary to ensure that only 1 set of values can fit the data by running the fitting optimisation with a wide range of guess values such that all the optimisations converge toward the same solution (**Note S11**).

Under high excitation fluences (*i.e.* $N_0 \gg N_T$, here $N_0 > 6 \times 10^{15}\ cm^{-3}$), the trap states are immediately saturated and most carriers undergo bimolecular recombination leading to dominant bimolecular contribution (**Figure 4c**). If the doping concentration is much lower than the photoexcited carrier concentrations, only the bimolecular rate constant can be accurately retrieved (**Notes S9** & **S11**).

Therefore, we advise to measure TRPL decays in the medium fluence regime where all the recombination processes are non-negligible. This regime can easily be identified by the fast initial drop of the TRPL intensity followed by a slower decay. TRPL decays measured in the low and high fluence regime can respectively be used to determine the product $k_T N_T$ and k_B. Furthermore, we recommend carrying out several fittings with different sets of guess values in order to confirm that only 1 set of values can fit the TRPL decay (**Note S11**).

Incomplete recombination

As previously discussed, experimental TRPL can only be fitted with a single excitation pulse by ensuring recombination of all the carriers between consecutive excitation pulses. As for the BT model, CA due to incomplete electron recombination can easily be avoided by ensuring that the TRPL intensity reaches zero, however, the BTD model predicts that trapped electrons can recombine non-radiatively after the free electron concentration, and therefore after the TPRL intensity, has reached zero. For example, in **Figure 5a** & **b** although both $RP = 100\ \mu s$ and $RP = 15\ \mu s$ allow recombination of most free electrons, $RP = 15\ \mu s$ does not allow all the trapped electrons and free holes to recombine before the next excitation pulse. The resulting TRPL after many consecutive excitation pulses shows a smaller initial decrease due to the presence of the trapped electrons, effectively reducing the available trap state concentration in the model (**Figure 5b** & **c**). Furthermore, the higher initial hole concentration affects bimolecular recombination.

Due to the non-radiative nature of trap-mediated recombination, CA of trapped electrons is more complicated to avoid than CA due to incomplete depopulation of the free electrons. The maximum difference between the single and multiple pulse TRPL decays was calculated at different excitation fluences for a repetition period chosen such that $I_{TRPL}(RP)/I_{TRPL}(0) = 10^{-4}$ (**Figure 5d**). Trap based CA does not affect the TRPL profile in the low fluence regime as the latter does not depend on the initial carrier concentration (however, if the initial carrier concentration becomes comparable to the trap state concentration, the TRPL profile then becomes dependent on the carrier concentration as shown in **Figure 5d**). In the high fluence regime, trap based CA is always negligible as trapping is also negligible compared to bimolecular recombination (**Figure 5d**). The highest difference due to CA is observed in the medium fluence regime. In this regime, it is possible to ensure complete depopulation of all trap states by gradually increasing the repetition period. Doing so allows more and more trapped electrons to detrap and the TRPL profile converges toward the single pulse TRPL profile (**Figure 5c**).

As for the BT model, the multiple pulse approximation can be used to fit TRPL decays subjected to CA. However, the higher occupation of the trap states limits the trapping contribution and thus may reduce the accuracy of the trapping rate constant and the trap state concentration retrieved (**Figure S9c**).

Our observations on the BTD model are summarised in **Table S2**.

ARTICLE View Article Online DOI: 10.1039/D0CP04950F

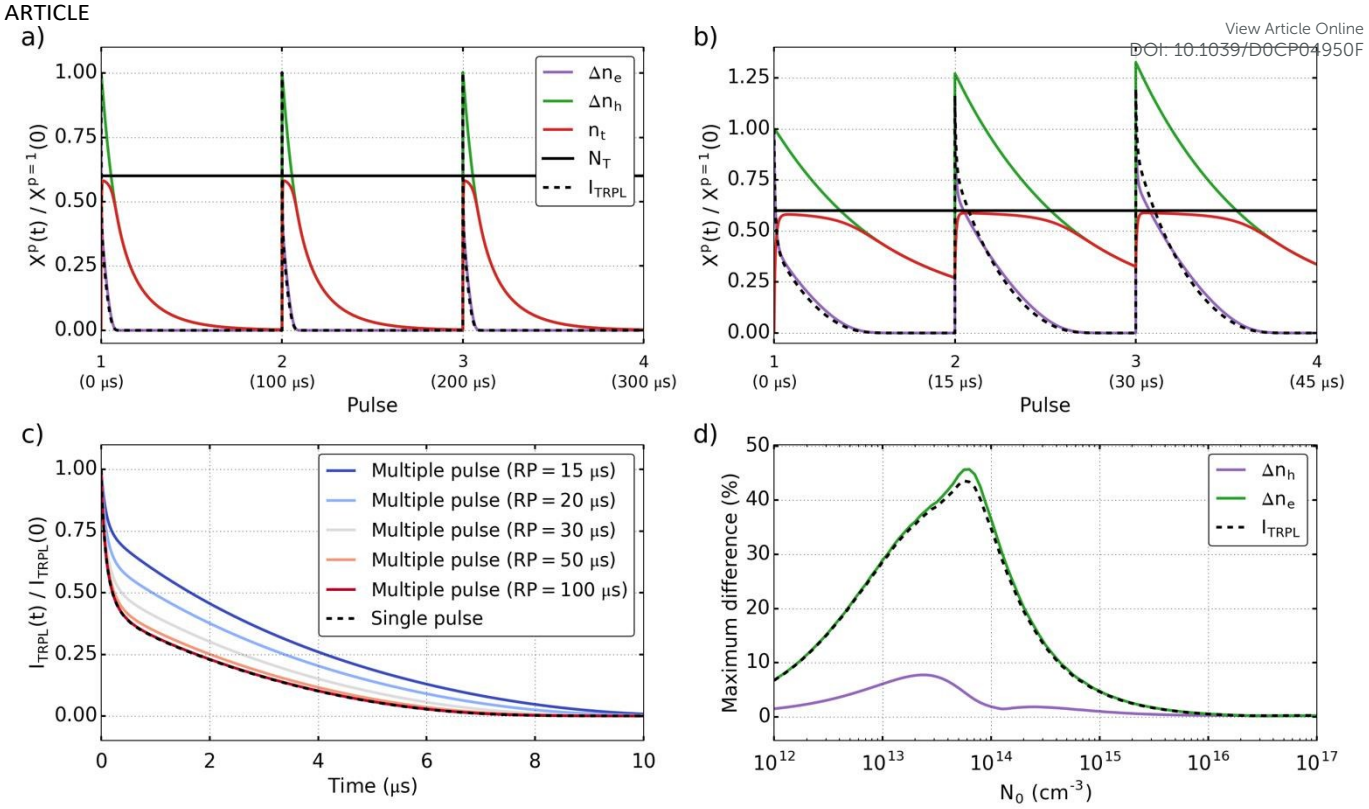

Figure 5: Evolution of the photoexcited electron Δn_e, hole Δn_h, trapped electron n_t concentrations and TRPL intensity I_{TRPL} as predicted by the bimolecular-trapping-detrapping model ($N_0 = 10^{14}\ cm^{-3}$) over 3 consecutive excitation pulses for a **a)** $RP = 100\ \mu s$ repetition period leading to negligible carrier accumulation and a **b)** $RP = 15\ \mu s$ repetition period leading to non-negligible carrier accumulation ($X = \Delta n_e, \Delta n_h, n_t, I_{TRPL}$). **c)** Normalised TRPL decays after multiple excitation pulses for different excitation repetition periods, compared to the TRPL after the first excitation pulse (single pulse). **d)** Maximum difference between the single pulse and multiple pulse normalised TRPL and carrier concentration decays at increasing N_0 (the repetition period was chosen such that $I_{TRPL}(RP)/I_{TRPL(0)} \sim 10^{-4}$).

Determination of the doping concentration

Although the absolute intensity measured by TCSPC is not usable due to the unknown ratio between the number of photons measured and photons emitted, it can still potentially be used to determine the doping concentration of the system. The experimentally measured initial TRPL intensity depends upon the initial carrier concentration (assuming negligible CA) and the doping concentration:

$$I_{TRPL}(0) \propto N_0(N_0 + p_0) \quad (34)$$

The doping concentration can be determined by measuring the initial TRPL intensity at two or more fluences N_0^A and N_0^B (**Note S13**):

$$p_0 = \frac{I_{TRPL}^B(0)P^A(N_0^A)^2 - I_{TRPL}^A(0)P^B(N_0^B)^2}{I_{TRPL}^A(0)P^B N_0^B - I_{TRPL}^B(0)P^A N_0^A} \quad (35)$$

where the number of pulses $\boldsymbol{P}$ can be calculated from the measurement time $\boldsymbol{M}$ and the repetition period:

$$\boldsymbol{P} = \frac{\boldsymbol{M}}{\boldsymbol{RP}} \quad (36)$$

Lifetime-based interpretation of TRPL

Interpretation of TRPL decays based on their lifetime is highly popular thanks to its simplicity. However, this method presents many limitations and drawbacks. Lifetime-based analysis does not consider the dependence of the recombination processes on the carrier concentration unlike the BT and BTD models. It can therefore only be used to compare samples measured with the same initial carrier concentration N_0, not subjected to any CA (as it affects the initial concentration) and presenting the same recombination processes (*e.g.* it is not possible to compare a perovskite film with and without contact with an electron transport layer as injection may happen in the latter). Furthermore, any observation made using this method is only valid for the initial carrier concentration used and may not be valid under solar cell operation for example. If these requirements are met and assuming that the electron and hole concentrations are equal at all time (as in the BT model), a longer overall lifetime of the TRPL indicates a longer lifetime of the free carriers and thus potentially a better efficiency of the perovskite when working in a complete device.

ARTICLE View Article Online DOI: 10.1039/D0CP04950F

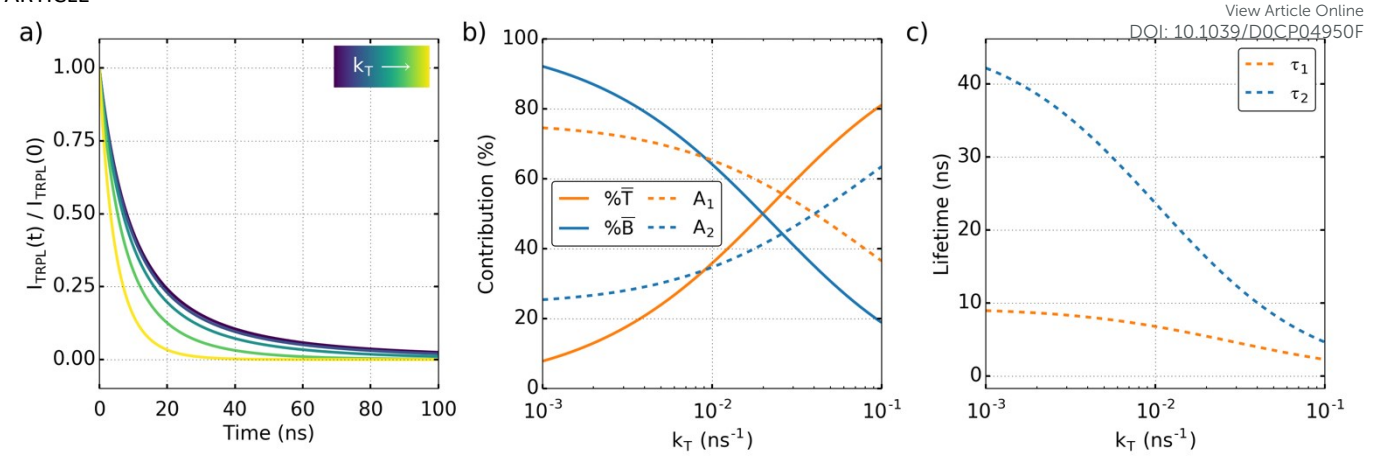

Figure 6: **Lifetime-based interpretation of TRPL decays. a)** TRPL decays simulated with the bimolecular-trapping model with increasing trapping rate constant k_T and **b)** corresponding total trapping $\%\overline{T}$ and bimolecular $\%\overline{B}$ contributions to the change in the carrier concentration. The amplitudes A_i and lifetimes τ_i obtained from bi-exponential fitting of the TRPL decays are shown in **b)** and **c)** respectively ($R^2 > 0.999$).

Multi-exponential models are usually used to quantify recombination processes by associating lifetimes with them. Here we discuss the suitability of this type of analysis by fitting TRPL decays simulated with the BT model with a bi-exponential function. Based on TRPL decays fitted with a bi-exponential function typical in literature, TRPL decays were simulated with the BT model with an increasing trapping rate constant (**Figure 6a**). The resulting amplitudes and lifetimes from bi-exponential fitting of these decays are reported in **Figure 6b & c**. The amplitude A_1 of the shorter exponential decreases while the amplitude A_2 of the longer component increases as the trapping rate constant increases. Considering the general assignment of the shorter component to trap-mediated recombination and the longer component with bimolecular recombination, the results of this fit could be interpretated as an increase of the contribution of bimolecular recombination and a decrease of the trapping contribution. However, this is inconsistent with our simulations as an increase of the trapping contribution and a decrease of the bimolecular contribution are predicted (**Figure 6b**). Although the decrease of the shorter lifetime τ_1 is consistent with the higher trapping rate, the decrease of τ_2 is inconsistent with the slower bimolecular rate due to lower carrier concentration induced by the higher trapping rate (**Figure 6c**). Bi-exponential fitting of TRPL decays can thus lead to misinterpretation of the processes occurring in the system studied and should therefore be used with scarcity.

Conclusions

Charge carrier recombination in perovskites is complex and as a result several models for charge dynamics have been used in the literature to extract meaningful data from TRPL decays. In this work, the limitations and fluence dependence of 2 charge carrier recombination models commonly used in the literature were reviewed. These models consider radiative and non-radiative bimolecular recombination, partially responsible for the dependence of the TRPL profile on the carrier concentrations, but differ in their treatment of trap-mediated recombination.

Both models predict dominant monomolecular trapping at low excitation fluence leading to a mono-exponential TRPL decay. Since other recombination processes are negligible in this regime, only trapping related information can be retrieved (that is the trapping rate constant k_T for the BT model and the product of the trapping rate constant and the trap state concentration $k_T N_T$ for the BTD model). Under high fluence, bimolecular recombination is dominant and only the bimolecular rate constant k_B can be accurately retrieved. Finally, in the medium fluence regime, the BT model predicts non-negligible trapping and bimolecular recombination allowing the accurate measurement of the rate constants of both processes. In the same regime, the BTD model predicts a fast initial trapping phase leading to a fast decrease of the TRPL intensity, which can be used to roughly determine the trap state concentration and trapping rate constant, followed by a slower decrease. The BTD model can be simplified by determining the values of some parameters beforehand; we propose a method to calculate the doping concentration from the initial TRPL intensity measured in the medium fluence regime. We demonstrate that the validity of the values retrieved from the BT model can be ensured by calculating the contribution of the processes to the change in the TRPL intensity. Due to the higher complexity of the BTD model, we advise ensuring that multiple sets of parameters' guess values for the fitting optimisation yield the same solution. We note that we limited this study on fitting single TRPL decays showing that it may be possible to accurately retrieve results from the model used in the medium fluence regime. However, we expect the accuracy of the results would be further improved by carrying out a global fitting of TRPL decays measured at different excitation fluences.

Incomplete depopulation of all photoexcited charge carriers within the excitation repetition period leads to an accumulation

of charge carriers in the system. This carrier accumulation usually happens over less than a few hundred excitation pulses and can alter the intensity and profile of the TRPL decay. Carrier accumulation due to incomplete electron recombination was found to be easily avoidable by choosing an excitation repetition period such that the TRPL intensity reaches zero. However, carrier accumulation due to incomplete detrapping as predicted by the BTD model only is harder to avoid as it can happen after the TRPL intensity has reached zero. In the medium fluence regime, complete detrapping can be ensured by comparing the TRPL decay profile measured with 2 excitation repetition periods. For both models, we showed that fitting TRPL decay subjected to carrier accumulation by simulating multiple pulses is possible but may be more limited than fitting TRPL decays presenting negligible carrier accumulation using single pulse fitting.

Finally, lifetime interpretation of TRPL of perovskites can only be used in specific cases and quantifying recombination processes using a multi-exponential fit may yield incorrect interpretations of the TRPL.

Both models discussed here have advantages and disadvantages: the BT model is a more simplistic approach of recombinations in perovskites but allows easy extraction of the process rate constants while the BTD model is more complex but requires more complex measurements in order to accurately retrieve the parameter values and avoid trap based carrier accumulation. Further processes can be considered in these models *e.g.* electron detrapping back the CB, Auger recombination and carrier diffusion. However, these processes will likely increase the complexity of the models and may require more complex measurements.

Due to the dependence of the TRPL on excitation fluence and excitation repetition period, we recommend these parameters be included in the experimental details of all published work.

We hope that this work will aid in the analysis of the TRPL of perovskite materials and will help the investigation of their complex and interesting properties.

Conflicts of interest

There are no conflict to declare.

Acknowledgements

We are grateful for the financial support of the EPSRC (EP/R016666/1 and EP/S001336/1) and both the EPSRC and Innovate UK for the SPECIFIC Innovation and Knowledge Centre and the European Regional Development Fund through the Welsh Government for support to the Sêr Solar program. MLD is grateful for funding through the EPSRC GCRF SUNRISE project (EP/P032591/1). We would like to acknowledge the assistance provided by the European Regional Development Fund through the Welsh Government (80708), the Ser Solar project via Welsh Government and Edinburgh Instruments.

References

1. National Renewable Energy Laboratory. Best Research-Cell Efficiency Chart | Photovoltaic Research | NREL [Internet]. National Renewable Energy Laboratory. 2019 [cited 2020 Sep 18]. Available from: https://www.nrel.gov/pv/cell-efficiency.html
2. Brenes R, Guo D, Osherov A, Noel NK, Eames C, Hutter EM, et al. Metal Halide Perovskite Polycrystalline Films Exhibiting Properties of Single Crystals. Joule [Internet]. 2017 Sep 6 [cited 2017 Dec 2];1(1):155–67. Available from: http://www.cell.com/joule/pdf/S2542-4351(17)30031-4.pdf
3. Motti SG, Meggiolaro D, Barker AJ, Mosconi E, Perini CAR, Ball JM, et al. Controlling competing photochemical reactions stabilizes perovskite solar cells. Nat Photonics [Internet]. 2019 May 27 [cited 2019 Jul 11];13(8):532–9. Available from: http://www.nature.com/articles/s41566-019-0435-1
4. Godding JSW, Ramadan AJ, Lin Y-H, Schutt K, Snaith HJ, Wenger B. Oxidative Passivation of Metal Halide Perovskites. Joule [Internet]. 2019 Nov 20 [cited 2020 Jul 20];3(11):2716–31. Available from: https://www.sciencedirect.com/science/article/abs/pii/S2542435119303812
5. Andaji-Garmaroudi Z, Anaya M, Pearson AJ, Stranks SD. Photobrightening in Lead Halide Perovskites: Observations, Mechanisms, and Future Potential. Adv Energy Mater [Internet]. 2020 Apr 1 [cited 2020 Aug 20];10(13):1903109. Available from: https://onlinelibrary.wiley.com/doi/abs/10.1002/aenm.201903109
6. Aristidou N, Eames C, Sanchez-Molina I, Bu X, Kosco J, Saiful Islam M, et al. Fast oxygen diffusion and iodide defects mediate oxygen-induced degradation of perovskite solar cells. Nat Commun [Internet]. 2017 May 11 [cited 2018 Mar 13];8:15218. Available from: http://www.nature.com/doifinder/10.1038/ncomms15218
7. Leguy A, Hu Y, Campoy-Quiles M, Alonso MI, Weber OJ, Azarhoosh P, et al. Reversible hydration of $CH_3NH_3PbI_3$ in films, single crystals and solar cells. Chem Mater [Internet]. 2015;27:3397–407. Available from: http://pubs.acs.org/doi/abs/10.1021/acs.chemmater.5b00660
8. Noomnarm U, Clegg RM. Fluorescence lifetimes: fundamentals and interpretations. Photosynth Res [Internet]. 2009 Sep 1 [cited 2019 Apr 4];101(2–3):181–94. Available from: http://www.ncbi.nlm.nih.gov/pubmed/19568954
9. Kirchartz T, Márquez JA, Stolterfoht M, Unold T. Photoluminescence-Based Characterization of Halide Perovskites for Photovoltaics. Adv Energy Mater [Internet]. 2020 May 6 [cited 2020 May 13];1904134. Available from: https://onlinelibrary.wiley.com/doi/abs/10.1002/aenm.201904134
10. Lakowicz JR. Principles of Fluorescence Spectroscopy [Internet]. Lakowicz JR, editor. Boston, MA: Springer US; 2006. Available from:

http://link.springer.com/10.1007/978-0-387-46312-4
11. De Melo JSS, Costa T, De Castro CS, Maçanita AL. Photophysics of fluorescently labeled oligomers and polymers. Photochemistry. 2013;41:59–126.
12. Zhang Z-YY, Wang H-YY, Zhang Y-XXY, Hao Y-WW, Sun C, Zhang Y-XXY, et al. The role of trap-assisted recombination in luminescent properties of organometal halide $CH_3NH_3PbBr_3$ perovskite films and quantum dots. Sci Rep [Internet]. 2016 Jul 1 [cited 2019 Apr 4];6(1):27286. Available from: http://www.nature.com/articles/srep27286
13. Du T, Kim J, Ngiam J, Xu S, Barnes PRF, Durrant JR, et al. Elucidating the Origins of Subgap Tail States and Open-Circuit Voltage in Methylammonium Lead Triiodide Perovskite Solar Cells. Adv Funct Mater [Internet]. 2018 Aug 1 [cited 2019 Mar 19];28(32):1801808. Available from: http://doi.wiley.com/10.1002/adfm.201801808
14. Yang J, Yu Y, Zeng L, Li Y, Pang Y, Huang F, et al. Effects of aromatic ammoniums on methyl ammonium lead iodide hybrid perovskite materials. J Nanomater [Internet]. 2017 Jan 12 [cited 2019 Apr 4];2017:1–6. Available from: https://www.hindawi.com/journals/jnm/2017/1640965/
15. Caprioglio P, Zu F, Wolff CM, Márquez Prieto JA, Stolterfoht M, Becker P, et al. High open circuit voltages in pin-type perovskite solar cells through strontium addition. Sustain Energy Fuels [Internet]. 2019 Jan 29 [cited 2019 Apr 4];3(2):550–63. Available from: http://xlink.rsc.org/?DOI=C8SE00509E
16. Yin J, Cao J, He X, Yuan S, Sun S, Li J, et al. Improved stability of perovskite solar cells in ambient air by controlling the mesoporous layer. J Mater Chem A [Internet]. 2015 Aug 4 [cited 2020 Apr 12];3(32):16860–6. Available from: http://xlink.rsc.org/?DOI=C5TA02843D
17. Liang P-W, Liao C-Y, Chueh C-C, Zuo F, Williams ST, Xin X-K, et al. Additive Enhanced Crystallization of Solution-Processed Perovskite for Highly Efficient Planar-Heterojunction Solar Cells. Adv Mater [Internet]. 2014 Jun 1 [cited 2020 Apr 12];26(22):3748–54. Available from: http://doi.wiley.com/10.1002/adma.201400231
18. Li Z, Dong J, Liu C, Guo J, Shen L, Guo W. Surface Passivation of Perovskite Solar Cells Toward Improved Efficiency and Stability. Nano-Micro Lett [Internet]. 2019 Dec 7 [cited 2020 Apr 12];11(1):50. Available from: http://link.springer.com/10.1007/s40820-019-0282-0
19. Hsiao K-C, Jao M-H, Li B-T, Lin T-H, Liao SH-C, Wu M-C, et al. Enhancing Efficiency and Stability of Hot Casting p–i–n Perovskite Solar Cell via Dipolar Ion Passivation. ACS Appl Energy Mater [Internet]. 2019 Jul 22 [cited 2020 Apr 12];2(7):4821–32. Available from: https://pubs.acs.org/doi/10.1021/acsaem.9b00486
20. Tao J, Ali N, Chen K, Huai Z, Sun Y, Fu G, et al. Enhanced efficiency in perovskite solar cells by eliminating the electron contact barrier between the metal electrode and electron transport layer. J Mater Chem A [Internet]. 2019 Jan 15 [cited 2020 Apr 12];7(3):1349–55. Available from: http://xlink.rsc.org/?DOI=C8TA10630D
21. Yao Z, Wang W, Shen H, Zhang Y, Luo Q, Yin X, et al. $CH_3NH_3PbI_3$ grain growth and interfacial properties in meso-structured perovskite solar cells fabricated by two-step deposition. Sci Technol Adv Mater [Internet]. 2017 Dec 31 [cited 2019 Apr 4];18(1):253–62. Available from: http://www.ncbi.nlm.nih.gov/pubmed/28458747
22. Yang Y, Ostrowski DP, France RM, Zhu K, van de Lagemaat J, Luther JM, et al. Observation of a hot-phonon bottleneck in lead-iodide perovskites. Nat Photonics [Internet]. 2016 Jan 26 [cited 2020 May 29];10(1):53–9. Available from: http://www.nature.com/articles/nphoton.2015.213
23. Herz LM. Charge-Carrier Dynamics in Organic-Inorganic Metal Halide Perovskites. Annu Rev Phys Chem [Internet]. 2016 May 27 [cited 2018 Aug 23];67(1):65–89. Available from: http://www.annualreviews.org/doi/10.1146/annurev-physchem-040215-112222
24. Yamada Y, Nakamura T, Endo M, Wakamiya A, Kanemitsu Y. Photocarrier recombination dynamics in perovskite $CH_3NH_3PbI_3$ for solar cell applications. J Am Chem Soc [Internet]. 2014 Aug 20 [cited 2018 Sep 1];136(33):11610–3. Available from: http://pubs.acs.org/doi/10.1021/ja506624n
25. Hutter EM, Eperon GE, Stranks SD, Savenije TJ. Charge Carriers in Planar and Meso-Structured Organic-Inorganic Perovskites: Mobilities, Lifetimes, and Concentrations of Trap States. J Phys Chem Lett [Internet]. 2015 Aug 6 [cited 2019 Apr 5];6(15):3082–90. Available from: http://pubs.acs.org/doi/10.1021/acs.jpclett.5b01361
26. Richter JM, Abdi-Jalebi M, Sadhanala A, Tabachnyk M, Rivett JPH, Pazos-Outón LM, et al. Enhancing photoluminescence yields in lead halide perovskites by photon recycling and light out-coupling. Nat Commun [Internet]. 2016 Dec 23 [cited 2019 Apr 29];7(1):13941. Available from: http://www.nature.com/articles/ncomms13941
27. deQuilettes DW, Frohna K, Emin D, Kirchartz T, Bulovic V, Ginger DS, et al. Charge-Carrier Recombination in Halide Perovskites. Chem Rev [Internet]. 2019 Sep 9 [cited 2019 Sep 10];acs.chemrev.9b00169. Available from: http://pubs.acs.org/doi/10.1021/acs.chemrev.9b00169
28. Crothers TW, Milot RL, Patel JB, Parrott ES, Schlipf J, Müller-Buschbaum P, et al. Photon Reabsorption Masks Intrinsic Bimolecular Charge-Carrier Recombination in $CH_3NH_3PbI_3$ Perovskite. Nano Lett [Internet]. 2017 Sep 13 [cited 2019 Sep 10];17(9):5782–9. Available from: https://pubs.acs.org/doi/10.1021/acs.nanolett.7b02834
29. Pazos-Outón LM, Szumilo M, Lamboll R, Richter JM, Crespo-Quesada M, Abdi-Jalebi M, et al. Photon recycling in lead iodide perovskite solar cells. Science

(80-) [Internet]. 2016 Mar 25 [cited 2019 Apr 4];351(6280):1430–3. Available from: http://science.sciencemag.org/content/351/6280/1430

30. Yamada Y, Yasuda H, Tayagaki T, Kanemitsu Y. Photocarrier recombination dynamics in highly excited $SrTiO_3$ studied by transient absorption and photoluminescence spectroscopy. Appl Phys Lett [Internet]. 2009 Sep 21 [cited 2019 Sep 19];95(12):121112. Available from: http://aip.scitation.org/doi/10.1063/1.3238269
31. Handa T, Tex DM, Shimazaki A, Wakamiya A, Kanemitsu Y. Charge Injection Mechanism at Heterointerfaces in $CH_3NH_3PbI_3$ Perovskite Solar Cells Revealed by Simultaneous Time-Resolved Photoluminescence and Photocurrent Measurements. J Phys Chem Lett [Internet]. 2017 Mar 2 [cited 2018 Aug 29];8(5):954–60. Available from: http://pubs.acs.org/doi/10.1021/acs.jpclett.6b02847
32. Kandada ARS, D'Innocenzo V, Lanzani G, Petrozza A. Chapter 4. Photophysics of Hybrid Perovskites. In: Unconventional Thin Film Photovoltaics [Internet]. Cambridge: Royal Society of Chemistry; 2016 [cited 2020 Sep 8]. p. 107–40. Available from: http://ebook.rsc.org/?DOI=10.1039/9781782624066-00107
33. Alnuaimi A, Almansouri I, Nayfeh A. Performance of planar heterojunction perovskite solar cells under light concentration. AIP Adv [Internet]. 2016 Nov 29 [cited 2020 Mar 16];6(11):115012. Available from: http://aip.scitation.org/doi/10.1063/1.4967429
34. Chirvony VS, González-Carrero S, Suárez I, Galian RE, Sessolo M, Bolink HJ, et al. Delayed Luminescence in Lead Halide Perovskite Nanocrystals. J Phys Chem C [Internet]. 2017 Jun 22;121(24):13381–90. Available from: https://doi.org/10.1021/acs.jpcc.7b03771
35. Chirvony VS, Martínez-Pastor JP. Trap-Limited Dynamics of Excited Carriers and Interpretation of the Photoluminescence Decay Kinetics in Metal Halide Perovskites. J Phys Chem Lett [Internet]. 2018 Sep 6;9(17):4955–62. Available from: https://doi.org/10.1021/acs.jpclett.8b01241
36. Yamada Y, Yasuda H, Tayagaki T, Kanemitsu Y. Temperature dependence of photoluminescence spectra of nondoped and electron-doped $SrTiO_3$: Crossover from auger recombination to single-carrier trapping. Phys Rev Lett [Internet]. 2009 Jun 18 [cited 2019 Sep 19];102(24):247401. Available from: http://www.ncbi.nlm.nih.gov/pubmed/19659046
37. Meggiolaro D, Motti SG, Mosconi E, Barker AJ, Ball J, Andrea Riccardo Perini C, et al. Iodine chemistry determines the defect tolerance of lead-halide perovskites. Energy Environ Sci [Internet]. 2018 Mar 14 [cited 2020 Jul 28];11(3):702–13. Available from: http://xlink.rsc.org/?DOI=C8EE00124C
38. Stranks SD, Burlakov VM, Leijtens T, Ball JM, Goriely A, Snaith HJ. Recombination Kinetics in Organic-Inorganic Perovskites: Excitons, Free Charge, and Subgap States. Phys Rev Appl [Internet]. 2014 Sep 11 [cited 2018 Jul 16];2(3):034007. Available from: https://link.aps.org/doi/10.1103/PhysRevApplied.2.034007
39. Savenije TJ, Guo D, Caselli VM, Hutter EM. Quantifying Charge-Carrier Mobilities and Recombination Rates in Metal Halide Perovskites from Time-Resolved Microwave Photoconductivity Measurements. Adv Energy Mater [Internet]. 2020 Jan 8 [cited 2020 Jan 9]; Available from: http://arxiv.org/abs/2001.02569
40. Li Y, Yan W, Li Y, Wang S, Wang W, Bian Z, et al. Direct Observation of Long Electron-Hole Diffusion Distance in $CH_3NH_3PbI_3$ Perovskite Thin Film. Sci Rep [Internet]. 2015 Nov 29 [cited 2019 Mar 29];5(1):14485. Available from: http://www.nature.com/articles/srep14485
41. Wehrenfennig C, Eperon GE, Johnston MB, Snaith HJ, Herz LM. High charge carrier mobilities and lifetimes in organolead trihalide perovskites. Adv Mater [Internet]. 2014 Mar 1 [cited 2019 Sep 13];26(10):1584–9. Available from: http://doi.wiley.com/10.1002/adma.201305172
42. Wu B, Nguyen HT, Ku Z, Han G, Giovanni D, Mathews N, et al. Discerning the Surface and Bulk Recombination Kinetics of Organic-Inorganic Halide Perovskite Single Crystals. Adv Energy Mater [Internet]. 2016 Jul 1 [cited 2019 Mar 4];6(14):1600551. Available from: http://doi.wiley.com/10.1002/aenm.201600551

View Article Online
DOI: 10.1039/D0CP04950F

Interpreting Time-Resolved Photoluminescence of Perovskite Materials

Emmanuel V. Péan[a], Stoichko Dimitrov[b], Catherine S. De Castro[c] and Matthew L. Davies[a,d]

Graphical abstract

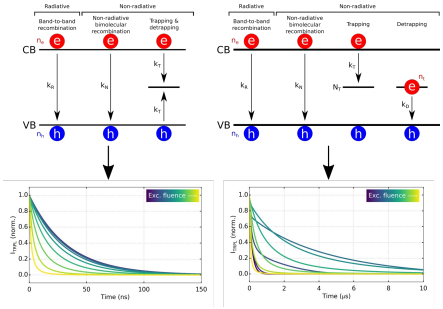

Evaluation of commonly used models to fit the TRPL of perovskites; retrieving meaningful data requires careful choice of excitation fluence.